

Effects of Natural Seawater and Electrochemical Potential on Fatigue-Crack Growth in 5086 and 5456 Aluminum Alloys

F. D. BOGAR

*NRL Marine Corrosion Research Laboratory
Key West, Florida*

and

T. W. CROOKER

*Metals Performance Branch
Engineering Materials Division*

October 7, 1977



NAVAL RESEARCH LABORATORY
Washington, D.C.

Approved for public release; distribution unlimited.

20. Abstract (Continued)

MPa·m^{1/2}. In ambient air, all four alloys exhibited similar crack growth characteristics. Crack growth in the 5086 alloys was only slightly affected by either seawater or potential. However, crack growth in the 5456 alloys varied rather widely with seawater and potential. In particular, alloy 5456-H116 exhibited crack-growth rates which were significantly accelerated at the freely corroding potential, and both 5456 alloys exhibited crack-growth rates which were significantly retarded under cathodic potentials. Observations of electrochemically induced crack arrest were made in both 5456 alloys under cathodic potential.

CONTENTS

INTRODUCTION	1
MATERIALS	1
EXPERIMENTAL DETAILS	2
RESULTS AND DISCUSSION	4
Ambient Air	4
Seawater — Freely Corroding	5
Seawater — Applied Potential	6
CONCLUSIONS	10
ACKNOWLEDGMENTS	11
REFERENCES	11
APPENDIX A — Crack-Growth Rate Data for 5086 and 5456 Aluminum Alloys	13



EFFECTS OF NATURAL SEAWATER AND ELECTROCHEMICAL POTENTIAL ON FATIGUE-CRACK GROWTH IN 5086 AND 5456 ALUMINUM ALLOYS

INTRODUCTION

5000-series aluminum alloys are among the leading candidate materials for application in advanced high-performance ship structures. Crack growth considerations will play a vital role in the development of criteria for materials selection, design, fabrication, inspection, and maintenance of these new ships [1].

However, to date, relatively little study has been devoted to the fatigue-crack growth characteristics of 5000-series marine aluminum alloys. The investigation reported here is an exploratory study on the effects of electrochemistry in corrosion-fatigue crack growth in this important class of naval alloys.

MATERIALS

The aluminum alloys studied in this investigation are 5086-H116, 5086-H117, 5456-H116, and 5456-H117. Aluminum alloys 5086 and 5456 are characterized by intermediate yield strength, high fracture toughness, good weldability, and high resistance to various forms of corrosion attack. Nominal compositions of these alloys are given in Table 1.

Table 1 — Nominal Chemical Compositions

Alloy	Element (wt-%)						
	Mn	Mg	Cr	Zn	Ti	Fe + Si	Cu
5086	0.2-0.7	3.5-4.5	0.25 max	0.25 max	—	0.90 max	0.10 max
5456	0.5-1.0	4.7-5.5	0.05-0.20	0.25 max	0.20 max	0.40 max	0.20 max

Note: Data from Alloy Digest, Engineering Alloys Digest, Inc., Upper Montclair, New Jersey

The H116 and H117 tempers were developed in recent years specifically to eliminate exfoliation in marine environments. Exfoliation in these alloys is thought to occur by a process of preferential corrosion through continuous networks of stringers consisting of precipitate particles. The H116 temper, developed by Reynolds Metals Co., seeks to avoid this undesirable condition through overaging, which tends to produce a uniform dispersion of fine particles and thus avoid continuous paths for exfoliation attack. The H117 temper, developed by the Aluminum Company of America, seeks to retain particle formers in solid

solution, thus producing a more uniform microstructure that results in somewhat higher fracture toughness than the H116 temper.

The alloys studied in this investigation were received as 25-mm-thick rolled plate. All tests were performed on the materials in the as-received condition. All tensile, fracture toughness, and fatigue-crack growth data reported are for crack paths oriented parallel to the final rolling direction in the T-L fracture plane orientation designated by ASTM [2].

Tensile properties measured on the selected materials (12.8-mm-diameter specimens) are given in Table 2. Fracture toughness data are plotted on a Fracture Resistance Diagram in Fig. 1. This diagram is a plot of fracture toughness vs yield strength, showing the upper and lower bounds of fracture toughness behavior for aluminum alloys as determined from extensive previous testing experience [3]. The diagram is subdivided into two regions on the basis of ASTM criteria for plane strain fracture toughness (K_{Ic}) in 25-mm-thick materials [4]. Below the ASTM-defined limit, 25-mm-thick aluminum alloys can be expected to undergo fracture in a brittle elastic manner. Above the limit, alloys can be expected to exhibit increasingly ductile elastic-plastic fracture behavior. In the uppermost regime of fracture toughness, 25-mm-thick alloys exhibit highly ductile, fully plastic fracture behavior. Although the four alloys studied in this investigation exhibited a rather broad range of fracture toughness, as determined by 25-mm dynamic tear tests [5], all of the fracture results for these materials fall well into the region of ductile elastic-plastic behavior as shown in Fig. 1.

Table 2 — Tensile Properties

Alloy	0.2% Offset Yield Strength (MPa)	Ultimate Tensile Strength (MPa)	Reduction of Area (%)	Elongation (%)
5086-H116	188	327	29.5	21.0
5086-H117	206	306	36.2	20.5
5456-H116	215	370	22.7	20.0
5456-H117	224	362	24.3	18.5

EXPERIMENTAL DETAILS

The fatigue tests described in this report were conducted at the Naval Research Laboratory's Marine Corrosion Research Laboratory in Key West, Florida. These tests were conducted using single-edge-notched (SEN) cantilever fracture mechanics specimens of the type shown in Fig. 2. Specimens were cycled under zero-to-tension loading, which is equivalent to a stress ratio of $R = 0$. Cyclic loads remained constant throughout each test. The cyclic frequency was 10 cpm (0.167 Hz).

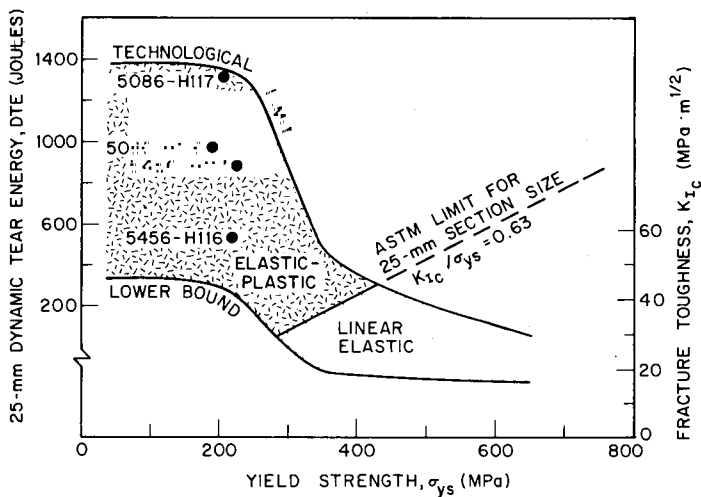


Fig. 1 — Fracture resistance diagram for aluminum alloys

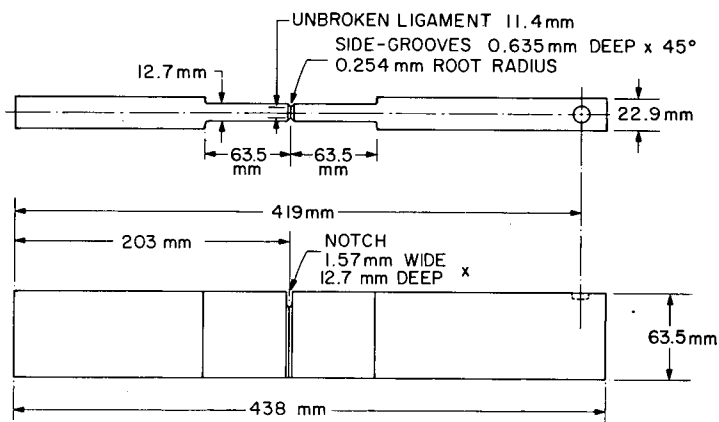


Fig. 2 — Details of the SEN cantilever specimen

Experimental observations consisted of regular periodic measurements of crack length (a) as a function of cycles (N). Crack length measurements were made optically using a Gaertner traveling micrometer focused on the crack tip. These a-vs-N plots were then graphically differentiated to produce plots of cyclic crack-growth rate (da/dN) vs the crack-tip stress-intensity range (ΔK). Stress-intensity calculations were performed using the Kies equation for notched bend bars [6].

Tests were conducted in ambient laboratory air and in fresh flowing natural seawater. The ambient laboratory air was controlled at approximately 50 percent relative humidity. The seawater was taken directly from the ocean at the laboratory site and immediately pumped through a polyurethane enclosure around the specimen test section in a single-pass mode at a flow rate of approximately 200 ml per min.

The corrosion-fatigue tests in natural seawater were conducted at the freely corroding (F.C.) potential, -0.955 V median value for the 5456 alloys and -0.975 V for the 5086 alloys, and at controlled potentials of -0.75, -1.3, -1.4 and -1.5 V. Potentials were controlled by means of a commercial potentiostat device and were measured against an Ag/AgCl reference electrode.

RESULTS AND DISCUSSION

Ambient Air

The fatigue-crack propagation characteristics of the four alloys studied, as determined in ambient air, are shown plotted in Fig. 3, which is a logarithmic plot of crack-growth rate (da/dN) vs stress-intensity range (ΔK). For the range of ΔK values studied ($\Delta K = 13$ to 41 $\text{MPa}\cdot\text{m}^{1/2}$), data for all four alloys fall on a common curve, which is distinctly sigmoidal in shape.

The data in Fig. 3 are in good agreement with prior results obtained by Chu on alloy 5456-H117 [7,8]. Chu also noted the sigmoidal shape of the logarithmic da/dN - ΔK curve, and he derived a modified form of the Forman equation [9] to express his results in the form

$$\frac{da}{dN} = C \frac{(\Delta K - \Delta K_{th})^n}{[(1 - R)K_c - \Delta K]^m}, \quad (1)$$

where R is the stress ratio (K_{min}/K_{max}), ΔK_{th} is the lower threshold for crack propagation, and K_c is the fracture toughness.

For expressing the data obtained in this study, two simplifications to equation (1) were possible: $R = 0$ and $m = 1$. Thus, for its application to the present study, equation (1) was reduced to the following form:

$$\frac{da}{dN} = C \frac{(\Delta K - \Delta K_{th})^n}{(K_c - \Delta K)}. \quad (2)$$

However, it must be strongly emphasized at this point that the values assigned to the parameters ΔK_{th} and K_c are only *apparent values* of these materials properties and thus serve only as fitting constants for the various trend line curves shown. For instance, the values of ΔK_{th} and K_c used to describe the data in Fig. 3 are 9.08 and 44.7 $\text{MPa}\cdot\text{m}^{1/2}$, respectively. As discussed by Bucci [10] and others [11, 12], actual ΔK_{th} values for aluminum alloys tend to lie well below the apparent value used to express the curve shown in Fig. 3. Similarly, the value of K_c used in the same equation is a misleading value of fracture toughness for these alloys. As illustrated in Fig. 1, under monotonic rising load, these 5000-series alloys are highly ductile and exhibit very high levels of fracture toughness, far in excess of the measurement capabilities of a linear-elastic fracture parameter such as K_c .

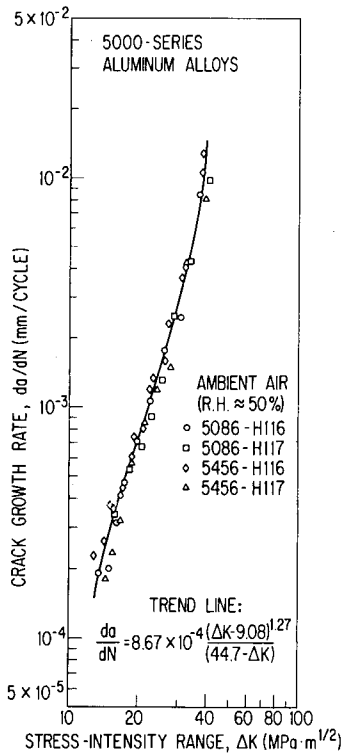


Fig. 3 — Fatigue-crack propagation characteristics of several 5000-series aluminum alloys in an ambient air environment

Overall, the results of this investigation are consistent with Chu's prior observations. That is, da/dN -vs- ΔK data for these alloys generated in several environments tend to suggest apparent ΔK_{th} values which are too high and apparent K_c values which are too low. The reasons for the excessively high ΔK_{th} values are not altogether clear. Recent studies [13] have shown that 5000-series aluminum alloys are susceptible to environmental effects on crack propagation as a function of relative humidity. Data presented in a later section of this report will show pronounced environmental effects on ΔK_{th} in some of these alloys as a function of applied potential. Therefore, environmental factors are a possible reason for the high apparent ΔK_{th} values reported here and in Chu's work.

An explanation for the excessively low K_c values is more readily apparent. In unpublished studies on alloy 5086-H116, Krafft et al. have analyzed this effect in relation to the cyclic strain-hardening characteristics of this alloy [14]. In effect, cyclic work-hardening transforms the ultimate fatigue-crack propagation resistance of these monotonically ductile alloys to much lower values normally associated with much more brittle, high-strength aluminum alloys.

Seawater — Freely Corroding

Crack-growth rate data obtained in flowing natural sea water under freely corroding conditions are shown in Fig. 4. The air environment trend line from Fig. 3 is included here for reference purposes. No significant sensitivity of crack-growth rates to seawater was noted

in these results except in the case of alloy 5456-H116. Previous observations of environmentally insensitive fatigue-crack growth in natural seawater or laboratory saline environments at low cyclic frequencies are quite rare and are considered to be a highly favorable characteristic for high-strength alloys intended for marine service. Previous alloys which fell into this category are 10Ni-Cr-Mo-Co and 9Ni-4Co-0.20C steels [15] and Ti-6Al-2Cb-1Ta-0.8Mo [16].

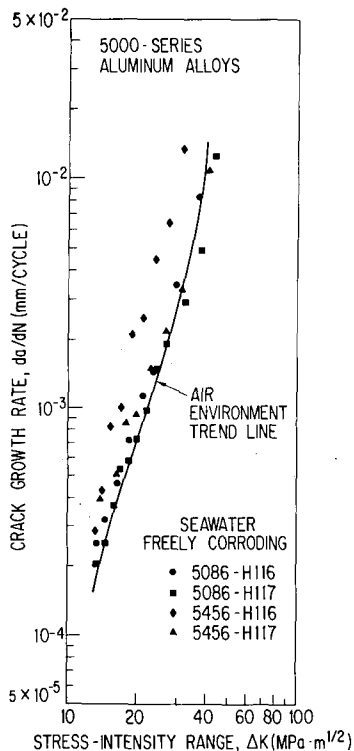


Fig. 4 — Fatigue-crack propagation characteristics of several 5000-series aluminum alloys in flowing natural sea-water under freely corroding conditions

In the mid-region of the ΔK values studied, da/dN values in 5456-H116 were increased by a factor of approximately three in response to the presence of seawater at freely corroding potential. Chu reported a doubling of crack-growth rates in alloy 5456-H117 in natural seawater [7]. A previous NRL study on alloy 5456-H321 showed crack-growth rates to be increased by as much as a factor of three in 3.5 percent NaCl saline solution [17]. Although these environmentally induced accelerations of 2 to 3 in crack-growth rates in 5000-series aluminum alloys are not insignificant, the environmental sensitivities noted here are far less than those for 7000-series aluminum alloys, which exhibit crack-growth rate accelerations of 5 to 20 under similar conditions [17,18].

Seawater — Applied Potential

Crack-growth rate data obtained in flowing natural seawater under applied potential are shown for each alloy studied in Figs. 5 through 8. In each case, trend lines based on equation 2 are shown for the freely corroding potential (~ 1.0 V) and for each applied potential. The values of the parameters C , n , ΔK_{th} and K_c used in each equation are tabulated in Table 3, and the values of all da/dN and ΔK data gathered in this study are tabulated in Appendix 1. For purposes of comparison, the reader is reminded that, with the exception of alloy 5456-H116 (Fig. 7), the air environment reference trend line is closely approximated by the freely corroding curve in seawater.

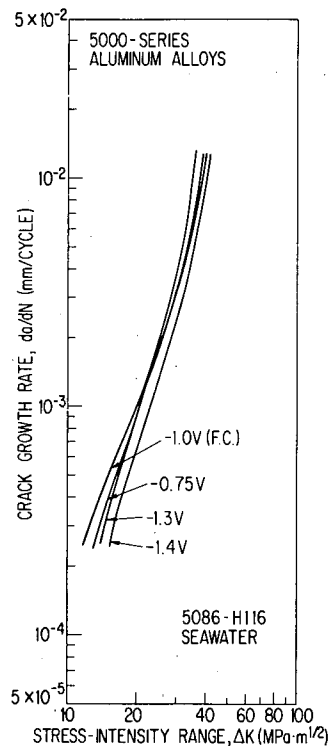


Fig. 5 — Effect of applied potential on fatigue-crack growth in 5086-H116 aluminum alloy in flowing natural seawater. Potentials are measured vs a Ag/AgCl reference electrode.

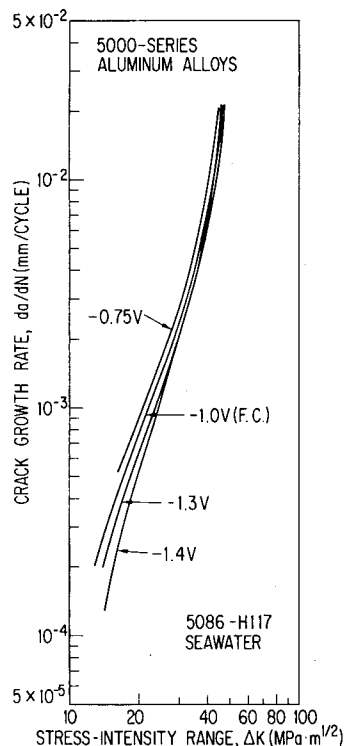


Fig. 6 — Effect of potential on fatigue-crack growth in 5086-H117 aluminum alloy in seawater

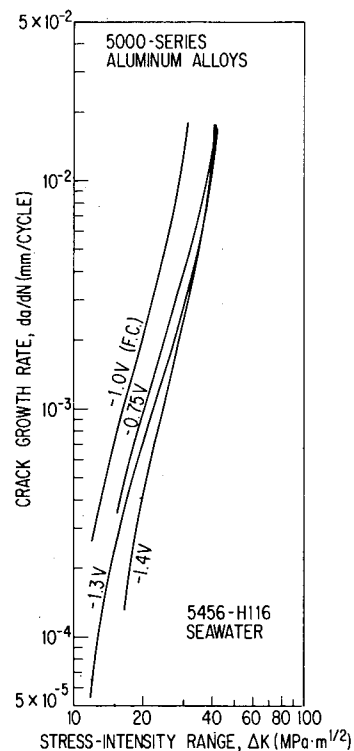


Fig. 7 — Effect of potential on fatigue-crack growth in 5456-H116 aluminum alloy in seawater

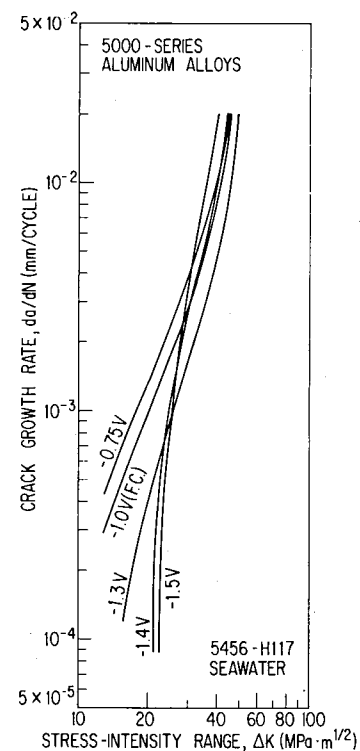


Fig. 8 — Effect of potential on fatigue-crack growth in 5456-H117 aluminum alloy in seawater

BOGAR AND CROOKER

Table 3 — Forman Equation Parameters

Alloy	Environment	Potential (V)	C	m	n	ΔK_{th} (MPa \sqrt{m})	K_c (MPa \sqrt{m})
5086-H116	Air	-	8.42×10^{-4}	1	1.27	9.2	45.3
	Seawater	F.C.	9.41×10^{-4}	1	1.27	8.0	44.9
	Seawater	-1.30	9.41×10^{-4}	1	1.27	9.7	40.7
	Seawater	-1.40	9.41×10^{-4}	1	1.27	10.1	47.3
	Seawater	-0.75	8.91×10^{-4}	1	1.27	6.0	45.7
5086-H117	Air	-	8.91×10^{-4}	1	1.27	8.8	48.3
	Seawater	F.C.	9.65×10^{-4}	1	1.28	7.7	51.6
	Seawater	-1.30	9.16×10^{-4}	1	1.27	8.8	51.6
	Seawater	-1.40	9.40×10^{-4}	1	1.28	10.7	50.5
	Seawater	-0.75	9.16×10^{-4}	1	1.27	6.2	48.8
5456-H116	Air	-	8.91×10^{-4}	1	1.27	8.9	44.2
	Seawater	F.C.	9.25×10^{-4}	1	1.45	8.2	36.3
	Seawater	-1.30	9.37×10^{-4}	1	1.32	10.2	47.3
	Seawater	-1.40	9.37×10^{-4}	1	1.32	13.7	45.1
	Seawater	-0.75	9.21×10^{-4}	1	1.50	9.7	51.4
5456-H117	Air	-	9.21×10^{-4}	1	1.40	10.4	53.0
	Seawater	F.C.	9.38×10^{-4}	1	1.30	6.2	49.5
	Seawater	-1.30	9.38×10^{-4}	1	1.30	12.0	54.4
	Seawater	-1.40	2.92×10^{-3}	1	1.45	18.7	65.5
	Seawater	-1.50	2.92×10^{-3}	1	1.45	21.0	51.3
	Seawater	-0.75	9.25×10^{-4}	1	1.45	5.2	54.8

The most pronounced feature of this collection of data is a nearly consistent trend toward lower crack-growth rates with increasingly negative potential. This trend is evident in all of the alloys, but is more pronounced in the 5456 alloys than in the 5086 alloys. Basically, the 5086 alloys were not strongly affected by either seawater or potential.

The most remarkable observations in this entire study were those indicating that crack-growth rates in seawater at cathodic potential were actually lower in many instances than those in ambient air at the same ΔK level and that an apparent electrochemically induced crack arrest could actually occur under these conditions. These observations are all the more remarkable because they stand in direct contrast with observations of very significant accelerations in crack-growth rates in steels under cathodic potentials [16,19].

An example of these effects of cathodic potential on crack growth is shown in Fig. 9, which is a plot of observed crack length (a) vs cycles of repeated load (N) for two specimens of alloy 5456-H117. Under freely corroding conditions, a specimen failed in approximately 28,000 cycles when cycled under constant load with an initial ΔK level of 13.8 MPa $\cdot m^{1/2}$. For the same alloy under potentiostatic conditions at -1.4 V vs Ag/AgCl and at an initial $\Delta K = 20.3$ MPa $\cdot m^{1/2}$, the specimen had not failed after 255,000 cycles and showed little evidence of significant crack extension.

In another experiment similar to that above, a crack was allowed to grow in 5456-H117 alloy under freely corroding conditions for a distance of 1.2 mm. At this point, with $\Delta K = 20$ MPa $\cdot m^{1/2}$, the specimen was polarized cathodically to -1.40 V and the crack growth was

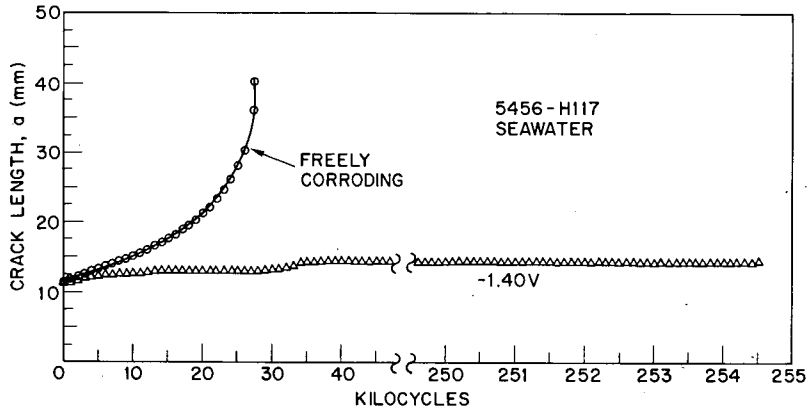


Fig. 9 — Crack length vs cycles data for alloy 5456-H117 in seawater showing crack growth to specimen failure in less than 30,000 cycles at the freely corroding potential and very limited crack growth after more than 250,000 cycles at -1.4 V

stopped. No further crack growth was observed for the next 275,000 cycles, after which the experiment was terminated. A microscopic examination of sections of the crack tip revealed no obvious features which would explain the lack of crack growth. In Fig. 10, a section of the crack tip of the 5456-H117 specimen etched with Keller's etch is shown at 100X. The large black precipitates are Mg_2Si , the gray precipitates are an $(Fe, Mn) Al_6$ complex, and the fine precipitates have been identified as Mg_2Al_3 . A fine precipitate banding is seen with accumulation at the grain boundaries. Cracking occurred along the grain boundaries; no significant bifurcation of the crack was observed.

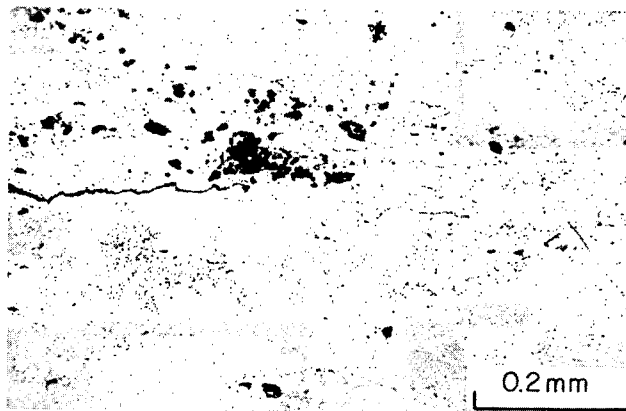


Fig. 10 — The crack tip at 100X for alloy 5456-H117 in seawater at -1.40 V vs. Ag/AgCl after more than 275,000 cycles at $\Delta K = 20 \text{ MPa}\cdot\text{m}^{1/2}$

The influences of electrochemical potential on crack-growth rates observed in this study are in general agreement with previous observations reported in the literature for aluminum alloys [20-22]. However, when comparisons are made with previously published results, attention should be focused on events at the lower regions of the curves in Figs. 5 through 8, since the observations cited in references 20-22 pertain to lower ΔK values than those encountered in the present study. Speidel et al. [20] studied the effect of specimen polarization on crack-growth rate in 7079-T651 aluminum at a single level of $\Delta K \approx 7 \text{ MPa}\cdot\text{m}^{1/2}$. They noted increasing values of da/dN with anodic potential and decreasing values of da/dN with cathodic potential, similar to what is found among the data for the 5086-H117 and 5456-H117 alloys at the lower ΔK values studied (Figs. 6 and 8). Dresty and Devereux [21] reported similar observation on 7075-T6 aluminum at ΔK values in the range of approximately 5 to 8 $\text{MPa}\cdot\text{m}^{1/2}$. Endo et al. [22] studied the effects of cathodic potential on a high-strength Al-Zn-Mg alloy. They observed crack-growth rates via post-failure striation spacing measurements. Their observations suggest that a minimum in da/dN is reached at potentials near -1.3 to -1.4 V, followed by a significant increase in da/dN at more negative potentials. None of the authors cited above reported electrochemically induced crack arrest of the type observed in the present study under cathodic potential.

CONCLUSIONS

The following conclusions were reached from this exploratory study.

- In an ambient air environment containing approximately 50 percent relative humidity, the fatigue-crack propagation characteristics of alloys 5086-H116, 5086-H117, 5456-H116 and 5456-H117 are essentially identical.
- In flowing natural seawater under freely corroding conditions, fatigue-crack growth rates in alloys 5086-H116, 5086-H117 and 5456-H117 showed no significant change from those measured in air. However, under these conditions, crack-growth rates in alloy 5456-H116 were as much as three times faster than those in air.
- In flowing seawater at an anodic potential of -0.75 V, crack-growth rates in the H117 temper alloys were slightly accelerated as compared to those measured at the freely corroding potential of -1.0 V, and crack-growth rates were slightly reduced in the 5086-H116 alloy at this anodic potential. Alloy 5456-H116 followed the same pattern of behavior; however, the reduction in crack-growth rates with anodic potential was of a more significant magnitude.
- In flowing natural seawater at cathodic potentials, which varied between -1.3 and -1.5 V, crack-growth rates in all four alloys tended to be reduced, especially at the lower ΔK values studied (~ 12 to $20 \text{ MPa}\cdot\text{m}^{1/2}$). This trend effect was much more pronounced in the 5456 alloys, which under these conditions had crack-growth rates that were actually lower than those measured in ambient air at the same ΔK levels.
- Overall, crack-growth rates in the 5086 alloys were not strongly affected by either seawater or applied potential.

• Observations of electrochemically induced crack arrest were made in the 5456 alloys in seawater at an applied cathodic potential of -1.4 V. Subsequent metallurgical examination revealed crack growth to be transgranular, and no evidence of crack branching could be detected.

ACKNOWLEDGMENTS

The authors acknowledge the valuable assistance of Mr. C.W. Billow and Dr. G.R. Yoder in conducting tests and interpreting results. The Office of Naval Research provided financial support for this study. The materials studied were donated by the Aluminum Company of America and the Reynolds Metals Company.

REFERENCES

1. H.H. Vanderveldt, T.W. Crooker, and J.A. Corrado, "Structural Integrity Technology for Advanced Surface Ships," *Naval Eng. J.* **88**, (No. 2), 97-104 (Apr. 1976).
2. R.J. Goode, "Identification of Fracture Plane Orientation," *Mater. Res. Standards*, **12** (No. 9), 31-32 (Sept. 1972).
3. R.J. Goode and R.W. Judy, Jr., "Fracture-Safe Design of Aluminum and Titanium Alloy Structures," NRL Report 7281, Feb. 14, 1972.
4. "Standard Method of Test for Plane-Strain Fracture Toughness of Metallic Materials," E399-74, in *1975 Annual Book of ASTM Standards*, Part 10, p. 561, American Society for Testing and Materials, Philadelphia, Pa., 1975.
5. P.P. Puzak and E.A. Lange, "Standard Method for the 1-Inch Dynamic Tear Test," NRL Report 6851, Feb. 13, 1969.
6. J.A. Kies, H.L. Smith, H.E. Romine, and H. Bernstien, "Fracture Testing of Weldments," *Fracture Toughness Testing and Its Applications*, ASTM STP 381, American Society for Testing and Materials, Philadelphia, Pa., 1965, pp. 328-353.
7. H.P. Chu, "Fatigue Crack Propagation in a 5456-H117 Aluminum Alloy in Air and Sea Water," *ASME Trans. J. Engrg. Mater. Technol.* **96**, Series H (No. 4), pp. 261-267 (Oct. 1974)
8. H.P. Chu, "Effect of Mean Stress Intensity on Fatigue Crack Growth in a 5456-H117 Aluminum Alloy," *Fracture Toughness and Slow-Stable Cracking*, ASTM STP 559, American Society for Testing and Materials, Philadelphia, Pa., 1974, pp. 245-263.
9. R.G. Forman, V.E. Kearney, and R.M. Engle, "Numerical Analysis of Crack Propagation in Cyclic-Loaded Structures," *ASME Trans., J. Basic Engrg.* **89**, Ser. D (No. 3), Sept 1967, pp. 459-464.

10. R.J. Bucci, discussion to paper by H.P. Chu, *Fracture Toughness and Slow-Stable Cracking* ASTM STP 559, 1974, pp. 261-262.
11. N.E. Frost, L.P. Pook, and K. Denton, "A Fracture Mechanics Analysis of Fatigue Crack Growth Data for Various Materials," *Engrg. Fracture Mech.* 3 (No. 2), Aug. 1971, pp. 109-126.
12. V. Weiss and D.N. Lal, "A Note on the Threshold Condition for Fatigue Crack Propagation," *Metal. Trans.* 5 (8), 1946-1949 (Aug. 1974).
13. R.L. Tobler and R.P. Reed, "Fracture Mechanics Parameters for 5083-0 Aluminum Alloy at Low Temperatures" (submitted to ASME Trans., *J. Engrg. Mater. Technol.*).
14. J.M. Krafft et al. Naval Research Laboratory, unpublished results.
15. T.W. Crooker and E.A. Lange, "Corrosion-Fatigue Crack Propagation Studies of Some New High Strength Structural Steels," *ASME Trans., J. Basic Engrg.* 91, Ser. D (No. 4), 570-574 (Dec. 1969).
16. T.W. Crooker, F.D. Bogar, and W.R. Cares, "Effects of Flowing Natural Seawater and Electrochemical Potential on Fatigue-Crack Growth in Several High-Strength Marine Alloys," NRL Report 8042, Aug. 30, 1976.
17. T.W. Crooker, "Fatigue and Corrosion-Fatigue Crack Propagation in Intermediate-Strength Aluminum Alloys," *ASME Trans., J. Engrg. Mater. Technol.* 95, Series H (No. 3), July 1973, pp. 150-156.
18. G.T. Hahn and R. Simon, "A Review of Fatigue Crack Growth in High Strength Aluminum Alloys and the Relevant Metallurgical Factors," *Eng. Fracture Mech.* 5 (No. 3), Sept. 1973, pp. 523-540.
19. O. Vosikovskiy, "Fatigue-Crack Growth in an X-65 Line-Pipe Steel at Low Cyclic Frequencies in Aqueous Environments," *ASME Trans., J. Engrg. Mater. Technol.* 97, Series H (No. 4), Oct. 1975, pp. 298-304.
20. M.O. Speidel, M.J. Blackburn, T.R. Beck, and J.A. Feeney, "Corrosion Fatigue and Stress Corrosion Crack Growth in High Strength Aluminum Alloys, Magnesium Alloys, and Titanium Alloys Exposed to Aqueous Solutions", *Corrosion Fatigue*, National Association of Corrosion Engineers, Houston, Texas, 1972, pp. 324-345.
21. J.E. Dresty and O.F. Devereux, "The Effect of Specimen Polarization on Fatigue Crack Growth Rates in 7075-T6 Aluminum", *Metal. Trans.*, 4 (No. 10), Oct. 1973, pp. 2469-2471.
22. K. Endo, K. Komai, and Y. Watase, "Cathodic Protection in Corrosion Fatigue of an Al-Zn-Mg Alloy", *Proc. 19th Japan Congr. Mater. Res.*, The Society of Materials Science, Japan, Kyoto, Japan, 1976, pp. 71-76.

Appendix A

CRACK-GROWTH RATE DATA FOR 5086 AND 5456 ALUMINUM ALLOYS

This appendix presents tables (Tables A1-A4) of crack-growth rate data for aluminum alloys 5086-H116, 5086-H117, 5456-H116, and 5456-H117 in air and seawater at various potentials. In each of the four tables environment and electrochemical potential are specified.

Table A1 — Crack-Growth Rate Data for Aluminum Alloy 5086-H116

Air		Seawater F.C.		Seawater -1.30 V		Seawater -1.40 V		Seawater -0.75 V	
ΔK (MPa $\sqrt{m}^{1/2}$)	(da/dN) (mm/cycle)	ΔK	(da/dN)	ΔK	(da/dN)	ΔK	(da/dN)	ΔK	(da/dN)
13.5	1.92 $\times 10^{-4}$	13.4	2.54 $\times 10^{-4}$	15.1	3.56 $\times 10^{-4}$	17.6	4.09 $\times 10^{-4}$	13.6	3.63 $\times 10^{-4}$
15.1	2.62 $\times 10^{-4}$	14.7	3.20 $\times 10^{-4}$	17.3	6.58 $\times 10^{-4}$	19.1	4.95 $\times 10^{-4}$	16.7	6.25 $\times 10^{-4}$
16.2	3.18 $\times 10^{-4}$	16.5	4.65 $\times 10^{-4}$	19.6	8.71 $\times 10^{-4}$	21.5	6.68 $\times 10^{-4}$	20.0	1.07 $\times 10^{-3}$
17.7	4.72 $\times 10^{-4}$	18.6	7.26 $\times 10^{-4}$	22.7	1.10 $\times 10^{-3}$	24.4	1.18 $\times 10^{-3}$	22.6	1.35 $\times 10^{-3}$
20.0	7.06 $\times 10^{-4}$	21.2	1.14 $\times 10^{-3}$	27.1	2.69 $\times 10^{-3}$	27.0	1.79 $\times 10^{-3}$	25.7	1.78 $\times 10^{-3}$
22.7	1.07 $\times 10^{-3}$	24.6	1.44 $\times 10^{-3}$	34.3	8.41 $\times 10^{-3}$	29.9	2.39 $\times 10^{-3}$	30.8	3.76 $\times 10^{-3}$
26.2	1.78 $\times 10^{-3}$	29.6	3.48 $\times 10^{-3}$			34.2	4.06 $\times 10^{-3}$	39.2	1.17 $\times 10^{-2}$
31.1	2.47 $\times 10^{-3}$	36.9	8.38 $\times 10^{-3}$			39.3	8.51 $\times 10^{-3}$		
37.5	8.51 $\times 10^{-3}$								

Table A2 — Data for Aluminum Alloy 5086-H117

Air		Seawater F.C.		Seawater -1.30V		Seawater -1.40 V		Seawater -1.40 V		Seawater -0.75 V	
ΔK (MPa $\sqrt{m}^{1/2}$)	(da/dN) (mm/cycle)	ΔK	(da/dN)	ΔK	(da/dN)	ΔK	(da/dN)	ΔK	(da/dN)	ΔK	(da/dN)
15.9	3.45 $\times 10^{-4}$	13.3	2.06 $\times 10^{-4}$	14.1	2.41 $\times 10^{-4}$	14.9	1.51 $\times 10^{-4}$	17.4	2.92 $\times 10^{-4}$	14.3	5.28 $\times 10^{-4}$
18.6	5.38 $\times 10^{-4}$	14.7	2.53 $\times 10^{-4}$	15.6	2.79 $\times 10^{-4}$	16.3	2.03 $\times 10^{-4}$	18.6	3.30 $\times 10^{-4}$	17.4	6.43 $\times 10^{-4}$
20.8	6.73 $\times 10^{-4}$	15.9	3.73 $\times 10^{-4}$	17.4	3.91 $\times 10^{-4}$	17.4	2.92 $\times 10^{-4}$	20.2	4.60 $\times 10^{-4}$	20.2	9.58 $\times 10^{-4}$
23.1	9.17 $\times 10^{-4}$	16.8	5.38 $\times 10^{-4}$	18.8	4.57 $\times 10^{-4}$	18.4	4.50 $\times 10^{-4}$	21.9	6.68 $\times 10^{-4}$	24.3	1.47 $\times 10^{-3}$
25.7	1.32 $\times 10^{-3}$	18.4	5.89 $\times 10^{-4}$	19.7	6.68 $\times 10^{-4}$	20.1	5.74 $\times 10^{-4}$	23.7	9.14 $\times 10^{-4}$	29.3	2.69 $\times 10^{-3}$
29.1	2.49 $\times 10^{-3}$	20.1	7.34 $\times 10^{-4}$	22.5	9.35 $\times 10^{-4}$	24.3	1.19 $\times 10^{-3}$	26.3	1.46 $\times 10^{-3}$	34.8	4.01 $\times 10^{-3}$
34.3	4.32 $\times 10^{-3}$	21.9	9.91 $\times 10^{-4}$	25.7	1.13 $\times 10^{-3}$	29.7	1.99 $\times 10^{-3}$	29.8	2.24 $\times 10^{-3}$	44.1	1.92 $\times 10^{-2}$
41.4	9.75 $\times 10^{-3}$	23.8	1.44 $\times 10^{-3}$	29.2	2.43 $\times 10^{-3}$	35.8	4.32 $\times 10^{-3}$	35.2	4.34 $\times 10^{-3}$		
		26.9	1.93 $\times 10^{-3}$	34.2	3.18 $\times 10^{-3}$	45.6	1.56 $\times 10^{-2}$	42.9	9.53 $\times 10^{-3}$		
		32.5	2.95 $\times 10^{-3}$	43.1	1.01 $\times 10^{-2}$						
		37.7	4.95 $\times 10^{-3}$								
		43.4	1.26 $\times 10^{-3}$								

Table A3 — Data for Aluminum Alloy 5456-H116

Air		Air		Seawater F.C.		Seawater -1.30 V		Seawater -1.30 V		Seawater -1.40 V		Seawater -0.75 V	
ΔK (MPa·m ^{1/2})	(da/dN) (mm/cycle)	ΔK	(da/dN)	ΔK	(da/dN)	ΔK	(da/dN)	ΔK	(da/dN)	ΔK	(da/dN)	ΔK	(da/dN)
12.9	2.29×10 ⁻⁴	15.4	3.68×10 ⁻⁴	13.2	2.90×10 ⁻⁴	12.5	4.78×10 ⁻⁵	15.4	3.30×10 ⁻⁴	16.8	1.51×10 ⁻⁴	15.7	4.60×10 ⁻⁴
14.3	2.64×10 ⁻⁴	16.9	4.17×10 ⁻⁴	14.2	4.34×10 ⁻⁴	12.6	6.12×10 ⁻⁵	17.1	3.89×10 ⁻⁴	18.5	2.21×10 ⁻⁴	17.6	5.18×10 ⁻⁴
15.7	3.63×10 ⁻⁴	18.9	6.15×10 ⁻⁴	15.4	8.28×10 ⁻⁴	13.3	1.32×10 ⁻⁴	18.5	5.38×10 ⁻⁴	20.2	3.91×10 ⁻⁴	19.3	9.32×10 ⁻⁴
17.3	4.47×10 ⁻⁴	21.2	8.08×10 ⁻⁴	17.1	1.01×10 ⁻³	14.3	2.11×10 ⁻⁴	20.1	8.31×10 ⁻⁴	22.9	6.48×10 ⁻⁴	21.9	1.20×10 ⁻³
19.3	7.52×10 ⁻⁴	23.5	1.35×10 ⁻³	19.1	2.12×10 ⁻³	16.2	3.35×10 ⁻⁴	22.2	1.21×10 ⁻³	23.6	1.39×10 ⁻³	25.4	2.17×10 ⁻³
22.6	1.20×10 ⁻³	27.3	2.33×10 ⁻³	21.3	2.49×10 ⁻³	23.5	9.68×10 ⁻⁴	26.3	1.73×10 ⁻³	31.6	3.23×10 ⁻³	27.6	3.40×10 ⁻³
26.4	1.60×10 ⁻³	32.4	4.06×10 ⁻³	24.1	4.50×10 ⁻³	25.3	1.70×10 ⁻³	30.9	2.92×10 ⁻³	39.3	1.19×10 ⁻²	41.4	1.64×10 ⁻²
31.3	3.66×10 ⁻³	38.2	1.06×10 ⁻²	27.3	6.48×10 ⁻³	28.8	2.01×10 ⁻³	35.1	4.70×10 ⁻³				
38.7	1.28×10 ⁻²			31.6	1.35×10 ⁻²	33.2	4.50×10 ⁻³	41.0	1.63×10 ⁻²				
						37.8	1.06×10 ⁻²						

Table A4 — Data for Aluminum Alloy 5456-H117

Air		Seawater F.C.		Seawater -1.30 V		Seawater -1.40 V		Seawater -1.50 V		Seawater -0.75 V	
ΔK (MPa·m ^{1/2})	(da/dN) (mm/cycle)	ΔK	(da/dN)	ΔK	(da/dN)	ΔK	(da/dN)	ΔK	(da/dN)	ΔK	(da/dN)
14.6	1.81×10 ⁻⁴	13.8	3.94×10 ⁻⁴	16.2	1.83×10 ⁻⁴	21.1	9.78×10 ⁻⁵	22.2	1.35×10 ⁻⁴	14.0	5.28×10 ⁻⁴
15.6	2.36×10 ⁻⁴	16.3	5.11×10 ⁻⁴	18.0	2.00×10 ⁻⁴	21.4	1.77×10 ⁻⁴	22.7	2.30×10 ⁻⁴	15.3	6.93×10 ⁻⁴
16.8	3.25×10 ⁻⁴	17.9	8.56×10 ⁻⁴	19.8	3.25×10 ⁻⁴	22.1	4.57×10 ⁻⁴	22.9	6.81×10 ⁻⁴	16.6	8.46×10 ⁻⁴
18.9	5.72×10 ⁻⁴	19.9	9.45×10 ⁻⁴	21.4	4.34×10 ⁻⁴	24.4	1.12×10 ⁻³	23.6	1.11×10 ⁻³	18.4	9.42×10 ⁻⁴
21.5	8.59×10 ⁻⁴	23.0	1.49×10 ⁻³	23.3	7.39×10 ⁻⁴	28.7	1.99×10 ⁻³	24.8	1.31×10 ⁻³	20.7	1.41×10 ⁻³
24.5	1.21×10 ⁻³	26.7	2.20×10 ⁻³	25.7	9.45×10 ⁻⁴	33.4	3.68×10 ⁻³	26.5	1.79×10 ⁻³	22.7	2.12×10 ⁻³
27.9	1.51×10 ⁻³	31.5	3.35×10 ⁻³	28.6	1.50×10 ⁻³	40.4	1.01×10 ⁻²	28.1	2.40×10 ⁻³	26.0	3.15×10 ⁻³
32.7	4.24×10 ⁻³	40.8	1.08×10 ⁻²	32.7	2.03×10 ⁻³			30.5	3.33×10 ⁻³	29.9	3.89×10 ⁻³
39.9	8.10×10 ⁻³			39.0	4.55×10 ⁻³			33.0	3.94×10 ⁻³		
				48.9	1.85×10 ⁻²			39.1	1.60×10 ⁻²		